Title

Inhibition of miR-29-3p isoforms via tough decoy suppresses osteoblast function in homeostasis but promotes intermittent parathyroid hormone-induced bone anabolism.

Authors

Hrdlicka, Henry
Pereira, Renata
Shin, Bongjin
et al.

Publication Date

2021-02-01

DOI

10.1016/j.bone.2020.115779

Peer reviewed

HHS Public Access

Author manuscript

Bone. Author manuscript; available in PMC 2022 February 01.

Published in final edited form as:

Bone. 2021 February ; 143: 115779. doi:10.1016/j.bone.2020.115779.

Inhibition of miR-29-3p isoforms via tough decoy suppresses osteoblast function in homeostasis but promotes intermittent parathyroid hormone-induced bone anabolism

Henry C. Hrdlicka[a], **Renata C. Pereira**[b], **Bongjin Shin**[c], **Siu-Pok Yee**[d], **Alix C. Deymier**[e], **Sun-Kyeong Lee**[c,**], **Anne M. Delany**[a,**]

[a]Center for Molecular Oncology, UConn Health Center, Farmington, Connecticut

[b]Division of Pediatric Nephrology, David Geffen School of Medicine at University of California, Los Angeles

[c]Center on Aging, UConn Health Center, Farmington, Connecticut

[d]Center for Mouse Genome Modification, UConn Health Center, Farmington, Connecticut

[e]Institute of Material Sciences, UConn Health Center, Farmington, Connecticut

Abstract

miRNAs play a vital role in post-transcriptional regulation of gene expression in osteoblasts and osteoclasts, and the miR-29 family is expressed in both lineages. Using mice globally expressing a miR-29-3p tough decoy, we demonstrated a modest 30–60% decrease all three miR-29-3p isoforms: miR-29a, miR-29b, and miR-29c. While the miR-29-3p decoy did not impact osteoclast number or function, the tough decoy decreased bone formation in growing mice, which led to decreased trabecular bone volume in mature animals. These data support previous in vitro studies suggesting that miR-29-3p is a positive regulator of osteoblast differentiation. In contrast, when mice were treated with intermittent parathyroid hormone (PTH1-34), inhibition of miR-29-3p augmented the effect of PTH on cortical bone anabolism, increased bone formation rate and osteoblast surface, and increased levels of Ctnnb1/βcatenin mRNA, which is a miR-29 target. These findings highlight differences in the mechanisms controlling basal level bone formation and bone formation induced by intermittent PTH. Overall, the global miR-29-3p tough decoy model represents a modest loss-of-function, which could be a relevant tool for assessing the possible

**Co-authors to whom correspondence should be addressed: Anne Delany, adelany@uchc.edu, Center for Molecular Oncology, UConn Health, 263 Farmington Ave, Farmington, CT 06030, Sun-Kyeong Lee, slee@uchc.edu, Center on Aging, UConn Health, 263 Farmington Ave, Farmington, CT 06030.

Author Contributions.

HCH: Investigation, Visualization, Writing-Original Draft. **RCP:** Investigation, Visualization; Writing-Review & Editing **BS**: Investigation, Validation. **SPY**: Methodology. **ACD**: Investigation. **SKL**: Conceptualization, Project Administration, Funding Acquisition, Writing-Review & Editing. **AMD**: Conceptualization, Methodology, Project Administration, Funding Acquisition, Writing-Review & Editing.

Disclosure statement.

The authors declare that they have no potential conflicts of interest.

impact of systemically administered miR-29-3p inhibitors. Our studies provide a potential rationale for co-administration of PTH1-34 and miR-29-3p inhibitors, to boost bone formation in severely affected osteoporosis patients, particularly in the cortical compartment.

Keywords

miRNA-29; tough decoy; osteoclast; osteoblast; bone formation; PTH

1. Introduction

The skeleton is a dynamic organ that continuously remodels through the coupled processes of bone resorption and bone formation (1). Bone homeostasis is dependent on the coordinated efforts of both hematopoietic and mesenchymal lineage cells. Bone marrow monocytes (BMMs) are hematopoietic lineage cells that can differentiate into multinucleated bone-resorbing osteoclasts, while bone marrow stromal cells (BMSCs) of the mesenchymal lineage can differentiate into bone-forming osteoblasts. A balance between osteoclast and osteoblast number and activity is needed for normal bone remodeling (1, 2).

microRNAs (miRNAs; miRs) are small, single-stranded, non-coding RNAs that post-transcriptionally fine-tune gene expression. This class of small RNAs are now well-recognized as an important regulator of both osteoclast and osteoblast lineages (3–7). miRNA-mediated regulation is achieved by incorporation of the mature miRNA strand into the multiprotein RNA-induced silencing complex (RISC), which targets mRNA transcripts with sequences complementary to the miRNA. RISC-miRNA:mRNA interactions can result in translational repression, transcript de-stabilization, and/or transcript degradation (1). Further, individual miRNAs frequently target multiple components of signaling pathways, resulting in wide-ranging regulation of cellular differentiation and function (7). One miRNA family shown to play a substantial role in the differentiation and function of osteoblasts and osteoclasts is miRNA-29-3p, an evolutionarily conserved family consisting of the isoforms: miR-29a-3p, -29b-3p, and -29c-3p (3–6, 8).

In the osteoclast lineage, we and others previously reported that the miR-29-3p family is up regulated in primary BMMs during macrophage colony stimulating factor (M-CSF) and receptor activator of NFκB ligand (RANKL) induced osteoclastogenesis (3, 9). We showed that inhibition of miR-29-3p activity decreases osteoclast formation, indicating the miR-29 family is a positive regulator of osteoclast differentiation (3). The miR-29-3p family promotes osteoclast differentiation and function, in part, by targeting *Gpr85*, *Cd93*, and *Nfia*, which negatively impact the commitment of BMMs to the osteoclast lineage, and by targeting *Calcr*, which mediates the anti-resorptive effects of calcitonin. Inhibition of miR-29-3p activity also decreased osteoclast precursor motility, which can impact osteoclast size (3).

In the osteoblast lineage, we and others previously reported that expression of the miR-29-3p family is increased with osteoblastic differentiation and that it positively regulates osteoblastogenesis and function in both mouse and human cells (5, 10–13). Upregulation of the miR-29-3p family promotes osteoblastogenesis, in part, by targeting

negative regulators of differentiation, including Hdac4, Tgfb3, and several negative regulators of Wnt-signaling (5, 10–13).

To date, the majority of studies investigating the function of the miR-29-3p family in bone were performed *in vitro*. To better understand the function of the miR-29-3p family *in vivo*, we developed a mouse model globally expressing a miR-29-3p tough decoy (miR-29 decoy; global decoy), which serves as a competitive inhibitor of miR-29-3p activity (14–16). In the present study, we show that under homeostatic conditions, decreased miR-29-3p activity impaired bone formation, leading to decreased trabecular bone volume, while osteoclastic parameters were unaffected. Unexpectedly, when challenged with intermittent PTH administration, the fold increase in osteoblast surface and bone formation rate were increased in miR-29 decoy mice compared with controls, an effect that could be related to increased βcatenin signaling. Overall, our data show a differential role for miR-29-3p in bone homeostasis and PTH-mediated bone anabolism.

2. Materials and Methods

2.1. Animal care

All animal protocols were approved by the Institutional Animal Care Committee at UConn Health. Mice were generated in the C57BL/6 background and were housed in the Center for Comparative Medicine at UConn Health. Animals were kept under a 12-h light/dark cycle and were provided with standard mouse chow and water *ad libidum*. Except when otherwise noted, female littermates were used for all experiments. Mice from several litters were pooled to generate enough individuals for each analysis. To evaluate bone formation via dynamic histomorphometry, mice were injected with 10 mg/kg calcein (Sigma) 7 and 2 days prior to the euthanasia of two-month-old animals, and 10 and 3 days prior to the euthanasia of six-month-old animals. To study bone-anabolic response, 12-week old mice were injected subcutaneously with 80 μg/kg/day rhPTH (1–34) (PTH) (Bachem, Torrance, CA) or vehicle alone (2% heat inactivated mouse serum in acidified saline), 5 days per week for 4 weeks (17, 18).

2.2. Generation of conditional miR-29 decoy allele

A miRNA tough decoy consists of a hairpin with an internal bulge containing two imperfect miRNA binding sites. The imperfection in the miRNA binding site (between bases 10 and 11 from the 3’ end of the complementary sequence) allows escape from RISC-mediated cleavage (15, 16, 19, 20). These decoys decrease the abundance of target miRNAs, as well as sequester the target miRNAs by acting as competitive inhibitors. A Rosa26-specific donor vector containing the tdTomato coding sequence followed by three-copies of a miR-29-3p tough decoy was prepared and used to generate the miR-29 decoy mouse line using CRISPR mediated gene editing. Supplemental Figures 1 and 2 provide additional details about generation of the construct and mice. The decoy was designed to interact with all miR-29-3p isoforms, with additional modifications to improve miRNA binding site accessibility.

A line of mice displaying germline transmission of the knock-in allele were bred with Hprt-Cre mice (Jax stock no: 004302; C57BL/6 background) to remove the STOP sequence (three

copies of the SV40 polyadenylation signal sequence), placing the tdTomato-miR-29-3p decoy under the transcriptional control of the CAG promoter, thus accomplishing global overexpression. Mice heterozygous for the globally expressed miR-29 decoy were crossed with each other and the genotype of the resulting pups was determined by PCR. Genotyping primers can be found in Supplemental Table 1. Wild-type mice and littermates homozygous for the decoy allele were retained for analysis.

2.3. Static and dynamic histomorphometry

For static histomorphometry, right femurs from global miR-29 decoy mice and littermate controls were fixed for 7 days in 4% paraformaldehyde at 4°C. After fixation, femurs were demineralized for 14 days in a 14% EDTA/2.7% NH_4OH solution. Femurs were subsequently dehydrated, paraffin embedded, and sectioned using a Leica microtome; 7 μm thick sections were stained for TRAP activity, with a hematoxylin counterstain.

For dynamic histomorphometry, left femurs were fixed 7 days in 4% paraformaldehyde at 4°C, incubated 24–36 hours in 30% sucrose, embedded in O.C.T. (Thermofisher) and flash frozen in super-cooled 2-methylbutane (Fisher); 7 μm sections were collected using a Leica cryostat and Cryofilm II tape transfer system (Section Lab Co. Ltd., Hiroshima, Japan). Sections were UV cross-linked to glass slides using Norland Optical Adhesive and mounted using 50% glycerol solution.

Static and dynamic histomorphometric parameters were measured using Osteomeasure software (OsteoMetrics) and were quantified 200 μm from the growth plate, avoiding cortices, as recommended by the Nomenclature Committee of the American Society for Bone and Mineral Research (21). Fluorescence and light micrographs were obtained using an Axiocam MRc digital camera and AxioVision software (Zeiss).

2.4. Micro-computed tomography (microCT)

Right femurs from global miR-29 decoy mice and littermate controls were fixed in 70% ethanol at 4°C until analysis. The metaphyseal region of the distal femur was analyzed at 8 μm voxel resolution using micro-CT (μCT40, Scanco Medical AG, Bassersdorf, Switzerland) to quantify trabecular and cortical microarchitecture (22).

2.5. Quantitative Real-time PCR (qPCR)

For whole bone gene expression, calvaria were cleaned of soft tissue, flash frozen, and homogenized in TRIzol reagent (Life Technologies); RNA was extracted as directed by the manufacturer. As previously described, total RNA was quantified, DNase treated (Promega), and subjected to random hexamer primed reverse transcription for Sybr green based quantitative PCR (qPCR) (4). For Sybr green based qPCR, gene expression was normalized to 18S rRNA. Primer sets are shown in Supplemental Table 1. miRNA levels were quantified using miRNA-specific TaqMan microRNA assays (Life Technologies). Briefly, miRNAs were reverse transcribed from total RNA using target-specific primers to create cDNA, which was quantified by qPCR. miRNA expression was normalized to RNU6B. Relative quantities were determined using standard curves and samples were assayed in duplicate. RNA from each mouse (biological replicate) was analyzed in duplicate (technical replicate).

2.6. Raman spectroscopy

To examine bone composition, Raman spectroscopy was performed on the cortical bone of femurs from five-month-old female mice (23). Briefly, 20 μm thick frozen sagittal sections of were analyzed using a Witec alpha 300 Raman system with a 785 nm^{-1} laser at an output power of 60–70 mW. Using a 100x objective, 5 measurements were collected along the long axis of the bone at the middiaphyseal region of the femoral cortex, approximately 20 μm apart.

Cosmic ray corrections and background subtractions were performed on all Raman spectra before analysis. Peaks of interest, including 960, 1000, 1070, 1451, and 1670 Δcm^{-1}, were fit as Lorentzian peaks using the Witec Control 5.1 fitting program. Starting parameters such as peak height and width were selected to obtain a visually determined best fit, after which the program was allowed to perform up to 200 fitting iterations to obtain a best fit. Peak center, width, and height for the five peaks of interest were recorded (23). Since Raman peak height can be affected by numerous factors, peak height ratios were reported in order to account for any scattering variations. The mineral to matrix ratio is represented as the ratio of the 960/1000 and 960/1670 peak height ratios and the mineral carbonate to phosphate ratio is represented by the 1070/960 peak height ratio.

2.7. Whole body adiposity

Whole body composition of lean and fat mass was measured using a minispec mq7.5 TD-NMR Analyzer (Bruker BioSpin Corporation, Billerca, MA, USA), according to manufacturer's instructions. A cohort of mice was analyzed longitudinally from two-months through six-months of age.

2.8. Statistics

Data shown in bar graphs are mean ± standard deviation. For data shown in box-and-whisker plots, the mid-line represents the median, the top and bottom of each box represents the 75% and 25% quartiles respectively, the whiskers mark the minimum and maximum values within the data set, and open circles represent outliers. Statistical significance was determined using ANOVA with Student-Newman-Keuls post-hoc test (KaleidaGraph, Synergy Software, Reading, PA).

3. Results

3.1. Generation of the global miR-29 decoy mice.

miR-29 family members are expressed from two loci in mouse: miR-29b-1 and miR-29a from chromosome 6, and miR-29c and miR-29b-2 from chromosome 1. The miR-29b loci give rise to identical miR-29b-3p isoforms. The miR-29-3p family members display remarkable sequence identity, such that miR-29a-3p and -29c-3p differ by a single nucleotide, whereas the 3'-end of miR-29b-3p shows more variation (Supplemental Figure 1). For all three isoforms, the seed binding region (bases 2–8), which is thought to nucleate interactions with mRNA targets, is identical (24–26). This suggests that miR-29-3p family members have the ability to target many of the same transcripts.

In an effort to inhibit the activity of the miR-29-3p family members, we designed a miR-29 tough decoy to serve as a competitive inhibitor for all three isoforms (**see** Supplemental Figure 1 **for decoy sequence**). We chose this strategy because it has been shown to be effective in knocking down the activity of miRNAs *in vivo* and *in vitro* (14–16). The decoy cassette consisted of the coding sequence for the fluorescent tdTomato reporter gene with three miR-29-3p tough decoys (each decoy containing 2 miR-29-3p binding sites) in its 3'-UTR. This decoy cassette was knocked into the Rosa26 locus such that its expression can be activated by Cre-mediated recombination of a floxed transcription stop consisting of three copies of the SV40 polyA signal (Supplemental Figure 2 and Figure 1A). A line of mice displaying germline transmission of the knock-in allele was crossed with HPRT-cre mice, resulting in global expression of the decoy cassette, demonstrated by ubiquitous tdTomato fluorescence in all tissues. Global miR-29 decoy mice were born at normal Mendelian ratios and were viable and fertile (data not shown). Frozen sections from long bones and calvaria (Figure 1B–D) demonstrated tdTomato fluorescence in all cells of the skeletal elements. qRT-PCR showed that tdTomato mRNA was well expressed calvaria of decoy animals, but was undetectable in wild type (data not shown). We also performed a limited survey of extraskeletal miR-29-expressing tissues, examining heart, kidney, liver and muscle. These tissues displayed tdTomato signal and were grossly normal upon histological analysis (Supplemental Figure 3).

Examining the expression of mature miR-29-3p by qRT-PCR, we found all three isoforms were significantly decreased (30–60%) in the calvaria of decoy animals compared to wild-type littermates (Figure 1E). In contrast, levels of two miRNAs normally expressed in both osteoclasts and osteoblasts, miR-30a-5p (group average Ct 24.2) and miR-365-3p (group average Ct 25.0), were unchanged (4, 27, 28). The impact of the miR-29-3p decoy was greatest for miR-29b-3p, the isoform known to be least stable (29). miR-29b-3p was also least abundant, evidenced by a higher group average Ct (28.1) compared with miR-29c-3p (average Ct 22.2) or miR-29a-3p (average Ct 24.1).

The miR-29-5p isoforms are not expected to interact with the decoy, since their mature sequence is not similar to that of the highly conserved −3p isoforms, and they are dissimilar to each other (Supplemental Figure 1). qRT-PCR showed that expression of miR-29c-5p (group average Ct 30.9) and miR-29b2-5p (group average Ct 37.8) were both significantly decreased in bone from miR-29-3p decoy mice, but miR-29a-5p (group average Ct 28.7) was not (Figure 1E). miR-29c and miR-29b2 are contained within the same primary miRNA, while miR-29a and miR-29b1 are contained within a different primary miRNA, transcribed from a different chromosome. Co-regulation of miR-29c-5p and miR-29b2–5p suggests that expression of the miR-29c/b2 locus, itself, may be decreased in miR-29-3p decoy mice. Further, compared with miR-29-3p, the relatively high average Ct values for the miR-29-5p isoforms indicate preferential selection for the −3p strand in bone. Moreover, miR-29a-3p and miR-29c-3p, being most abundant, are likely the predominant miR-29 regulatory entities in bone. Overall, our data suggest that expression of the decoy results in a modest but specific knockdown of miR-29-3p isoforms.

3.2. miR-29 decoy decreases bone formation at two-months of age.

We first assessed the microarchitecture of femoral trabecular and cortical bone at two-months of age, the time of peak trabecular bone volume in C57BL/6 mice (30). MicroCT analysis did not reveal a significant impact of the global miR-29 decoy on trabecular or cortical bone compartments in either male or female mice at this age (Supplemental Figure 4 and Figure 2).

However, since the miR-29 family positively regulates both osteoclast and osteoblast differentiation and function *in vitro*, histomorphometry and serum markers were used to examine cellular parameters of bone turnover in female mice *in vivo* (Figure 3). Regarding osteoclast parameters, static histomorphometry did not reveal a difference in osteoclast surface or eroded surface between wild-type and global decoy mice (Figure 3D and E). Although statistical significance was not achieved, serum CTX (marker of systemic bone resorption) trended higher in the decoy mice compared to wild-type (Figure 3F). Dynamic histomorphometry (Figure 3H and I) showed significantly decreased bone formation rate and mineralizing surface in global decoy mice compared to wild-type controls (Figure 3J and L). While statistical significance was not achieved, mineral apposition rate (Figure 3K) also trended lower in the decoy mice, as did osteoblast surface (Figure 3C). Serum P1NP (marker of systemic bone formation) was not altered in the decoy mice (Figure 3G). Together, these data suggest the major impact of the global miR-29 decoy in bone *in vivo* is occurring in the mesenchymal lineage.

To examine this more closely, we evaluated the expression of osteoblast markers genes *Runx2* (master transcription regulator of osteoblastogenesis) and *Bglap* (osteocalcin; an osteoblastic differentiation marker) in the calvaria of two-month old wild-type and global decoy mice. We observed a significant decrease in *Runx2* expression in global decoy mice, while *Bglap* only trended lower (Figure 4A and B). Together, dynamic histomorphometry and gene expression data indicate decreased osteoblast function in global decoy mice.

To further examine osteoblast function, we evaluated mRNA expression of *Rankl* (driver of osteoclastogenesis) and *Opg* (soluble RANKL decoy receptor). While *Rankl* was not changed, *Opg* was significantly decreased in the global decoy mice, resulting in an increased *Rankl/Opg* ratio (Figure 4C–E). While this increase in the *Rankl/Opg* ratio would suggest a pro-osteoclastic environment, significant alterations in osteoclast parameters were not observed at two months of age (Figure 3D and E).

3.3. Decreased trabecular bone volume in skeletally mature miR-29 decoy mice.

Although femoral trabecular and cortical bone microarchitecture were unaltered in two-month-old decoy mice, these mice displayed a robust decrease in bone formation rate. To determine whether this might contribute to differences in the skeleton of mature mice, we analyzed six-month-old animals (Figure 5). Although cortical bone parameters were not different at the level of microarchitecture (Figure 5G–I), alterations in bone matrix properties can have a significant impact on biomechanical properties. Therefore, Raman spectroscopy was used to determine cortical bone mineral-to-matrix ratio, which is a primary determinant of bone quality, as well as the carbonate-to-phosphate ratio. However,

significant differences in these ratios between wild-type and miR-29 decoy mice were not detected (Figure 5J, K). Unaltered cortical bone morphology, coupled with unaffected matrix properties, suggests that global expression of the miR-29-3p decoy does not affect bone strength.

While the miR-29 decoy did not alter cortical bone parameters in six-month-old mice, significant effects were observed in the trabecular compartment. Both bone-volume fraction (Figure 5C) and trabecular number (Figure 5E) were decreased in miR-29 decoy mice, whereas trabecular spacing (Figure 5D) was increased. Trabecular thickness (Figure 5F) and total bone volume (Figure 5B) were unaltered.

Histomorphometry and analysis of serum markers were used to determine if cellular parameters were altered at this age (Figure 6). Unlike the two-month-old animals, dynamic histomorphometric analysis of six-month-old mice did not reveal significant differences in mineralizing surface, bone formation rate, or mineral apposition rate between wild-type and global decoy animals (Figure 6H, K, and L); osteoblast surface and serum P1NP were also unchanged (Figure 6G and J). Similarly, osteoclast surface and eroded surface were not different between six-month-old wild-type and global decoy animals (Figure 6C and D). While serum CTX trended higher in the six-month decoy mice compared to wild-type, it did not achieve significance (Figure 6I). These data suggest that the decreased bone formation seen in two months of age translated to decreased trabecular bone volume at six months in the global decoy mice.

3.4. Global expression of the decoy does not affect adiposity.

The miR-29 family was previously reported to be downregulated during adipocyte differentiation and to negatively regulate this process, targeting several transcription factors needed for adipogenesis (31–35). To determine if global expression of the miR-29 decoy affected adiposity, we performed a longitudinal study of whole-body composition using TD-NMR (Supplemental Figure 5). Both wild-type and decoy mice showed significantly increased total mass from two- to six-months of age ($p<0.01$), which was not affected by genotype (Supplemental Figure 5A). Percent lean mass, and percent fat mass (Supplemental Figure 5B and C) remained similar from two to six months of age, and were also unaffected by genotype. These data suggest that, up to six-months of age, global expression of the miR-29 decoy does not impact whole body composition.

3.5 Increased osteoblast surface and bone formation in miR-29 decoy mice receiving intermittent PTH

Since global expression of the miR-29-3p decoy caused a decrease in bone formation in homeostasis, we hypothesized that the decoy mice would accrue less bone when subjected to intermittent administration of PTH1-34, a bone anabolic therapy currently used to treat patients severely affected by osteoporosis (36). To test this hypothesis, 12-week-old miR-29-3p decoy mice and littermate controls were injected with 80 μg/kg rhPTH1-34, 5 days per week, for 4 weeks prior to tissue harvest for microCT (Figure 7), histomorphometry (Figure 8), and RNA analysis (Figure 9). MicroCT showed that intermittent PTH increased cortical thickness in both miR-29 decoy mice and controls, an

effect driven by increased subperiosteal area in both genotypes (Figure 7G and I). However, the cortical thickness of PTH treated miR-29 decoy mice was modestly (~3%), but significantly higher than PTH treated wild types, suggesting an enhanced anabolic response in the decoy mice.

microCT analysis also demonstrated decreased trabecular bone volume fraction (BV/TV) in vehicle treated miR-29 decoy mice compared with vehicle treated controls, an effect consistent with observations at six-months of age (Figures 7C and 5G). Intermittent PTH caused a similar fold increase in bone volume fraction in mice of both genotypes (Figure 7C). However, PTH-mediated effects on the individual parameters of trabecular thickness, spacing or number were not observed at the level of microCT (Figure 7D–F). Nevertheless, static histomorphometry, which examines trabecular bone parameters at a higher resolution, revealed that PTH significantly increased trabecular number and thickness in both wild type and miR-29 decoy mice, while trabecular spacing was correspondingly decreased (Figure 8C–E). Static histomorphometry also showed that trabecular number was decreased in vehicle treated decoy mice compared with vehicle treated wild types, while trabecular spacing trended higher; this reinforces the concept that miR-29-3p inhibition has a negative impact on homeostatic bone balance (Figure 8C and E).

At the cellular level, static histomorphometry did not demonstrate a significant effect of PTH on osteoclast surface or eroded surface in mice of either genotype (Figure 8J and K). In contrast, osteoblast surface was increased by PTH in both wild type and miR-29 decoy mice, an effect that was significantly enhanced in decoy mice (Figure 8F). While PTH increased mineral apposition rate to a similar extent in mice of both genotypes, bone formation rate, which is adjusted for bone surface, was only significantly increased in miR-29 decoy mice (Figure 8H and I). Although adipocyte number was unaffected by PTH, this parameter trended higher in vehicle treated miR-29 decoy mice compared with vehicle treated wild type (Figure 8L). Overall, these data indicate that decreasing miR-29-3p activity increases the bone anabolic response to intermittent PTH by increasing osteoblast surface and bone formation rate.

This unexpected response of the miR-29 decoy mice to intermittent PTH led us to examine RNA levels for validated miR-29-3p targets that may have an impact on response to PTH bone. Ctnnb1/β-catenin RNA was previously shown to be increased in bone of mice treated with intermittent PTH, and Ctnnb1 is a recently validated miR-29-3p target (37–39). qRT-PCR confirmed that PTH increased Ctnnb1/β-catenin RNA in both wild type and miR-29 decoy mice, but this increase was significantly higher in the decoy mice (Figure 9A). In contrast, RNA for Bmpr1a/ALK3, another recently described miR-29-3p target, was not increased by PTH in wild type mice, but trended higher in PTH treated miR-29 decoy mice (Figure 9B) (37). These data suggest that canonical Wnt signaling, known to be important for the bone anabolic effects of intermittent PTH, may play a role in the ability of the miR-29-3p decoy to augment bone formation (36).

Lastly, we examined the effect of intermittent PTH treatment on miR-29-3p isoform expression in bone. qRT-PCR showed that PTH did not significantly alter the abundance of miR-29a-3p or miR-29c-3p, while miR-29b-3p trended higher in wild type mice (Figure

9C–E). Compared with wild type, all three miR-29-3p isoforms were significantly decreased in both vehicle and PTH treated miR-29 decoy mice, confirming activity of the decoy. Altogether, these data confirm that decreased miR-29-3p activity has a negative impact on bone balance in homeostasis, but increases the bone anabolic response to intermittent PTH by increasing osteoblast surface and bone formation rate. This positive effect of miR-29 inhibition on bone acquisition in response to PTH may, in part, involve β-catenin-mediated mechanisms.

4. Discussion

The interplay of osteoblasts and osteoclasts is integral for skeletal homeostasis, and miRNAs play a vital role in post-transcriptional regulation of gene expression in these bone cells (1). The miR-29 family is expressed in both osteoblast and osteoclast lineages. Using mice globally expressing a miR-29-3p tough decoy, we showed that a modest 30–60% decrease in miR-29-3p family members did not impact osteoclast number or function. However, expression of the decoy decreased bone formation in growing mice, which led to decreased trabecular bone volume in mature animals (Figures 1, 3, 5). These data support previous in vitro studies suggesting that miR-29-3p is positive regulator of osteoblast differentiation (5, 10, 13). In contrast, when miR-29 decoy mice were treated with intermittent PTH, cortical thickness was enhanced to a greater extent than in wild type, as was bone formation rate, osteoblast surface, and levels of Ctnnb1/β-catenin mRNA, which is a miR-29-3p target (Figures 7–9). These findings highlight differences in the mechanisms controlling basal level bone formation and bone formation induced by intermittent PTH.

In vitro studies using osteoblastic cell lines demonstrated that miR-29-3p is a positive regulator of osteoblastogenesis, targeting negative regulators of osteoblastic differentiation, including Hdac4, Tgfb3, and several Wnt signaling antagonists (5, 10–13). Somewhat paradoxically, the miR-29 family is also well-recognized for its ability to target extracellular matrix mRNAs, including those for type I collagens and for non-collagenous extracellular matrix components regulating fibril formation, mineralization, and the activity of specific growth factors (5, 11, 40, 41). *In vitro*, miR-29-3p levels are low in early osteoblasts, which are responsible for depositing large amounts of extracellular matrix. The expression of the miR-29-3p family members then increases as the matrix matures and becomes mineralized (11). These data suggest that the cell modulates miR-29 levels to promote the gene expression programs needed at different phases of osteoblastic differentiation program.

Although they are of the same lineage, the transcriptional profiles of osteoblasts and osteocytes display important distinctions (42). Due to the modular nature of miRNA-mediated regulation, the same miRNA may have different roles in different cell types, due to the complement of mRNA targets available for interaction. Like osteoblasts, miR-29b-3p family members are expressed in osteocytes, which are the most abundant cells in bone (43). It is possible that part of the bone anabolic effect of miR-29-3p inhibition in mice treated with intermittent PTH reflects an effect on osteocytes, which are critical for the response of the skeleton to PTH (44, 45). In osteocytes, PTH increases expression of RANKL while decreasing the paracrine Wnt inhibitor, SOST/sclerostin, which plays an important role in PTH-stimulated bone formation (36). PTH also increases osteocyte expression of the Wnt

co-receptor LRP6, which is needed for PTH-stimulated bone anabolism and β-catenin signaling (46, 47). Both β-catenin and Lrp6 are recently validated miR-29-3p targets (37). Enhanced levels of Ctnnb1/β-catenin mRNA in PTH treated miR-29 decoy mice (Figure 9A) could promote sensitivity to Wnt signaling (37).

Intriguingly, previously published RNA sequencing data suggest that PTH treatment might cause osteocytes to revert to a less differentiated phenotype, at least in vitro (48). For example, one study identified a subset of ~880 genes that were regulated both by the osteoblast to osteocyte transition and by PTH. However, the majority of those up regulated by PTH were down regulated by osteocytic differentiation, while the majority of those down regulated by PTH were up regulated during osteocyte differentiation (48). In wild type mice, miR-29-3p isoforms in bone were not significantly regulated by intermittent PTH in vivo (Figure 9C–D). However, decreased miR-29-3p levels, due to expression of the decoy, may have favored the adoption of a “less differentiated” phenotype associated with PTH treatment. Compared to osteoblasts and osteoclasts, the function of miRNAs in osteocytes is relatively unexplored. Understanding the function of miR-29-3p in osteocytes is an ongoing interest.

It is well established that miRNAs regulate the tempo and amplitude of gene expression programs. It is common for a miRNA to target multiple members within a signaling pathway, acting to balance or buffer signaling by participating in regulatory loops that are feed-forward, feed-back or incoherent (49, 50). In different cell systems, miR-29-3p family members have been shown to be either positive or negative regulators of Wnt signaling, directly targeting negative or positive modulators of the pathway (5, 10, 37, 51–54). Thus, it is likely that the overall impact of miR-29 on Wnt signaling reflects the complement of targets present within the cell at the time, as well as the levels of miR-29-3p isoforms themselves. These can change not only with stage of differentiation, but also with time of day, as miR-29-3p family members display circadian rhythm, at least in bone (4).

Although intermittent PTH did not significantly alter the levels of miR-29-3p in bone (Figure 9), miR-29-3p isoforms are regulated in some mouse models of bone disorders. For example, glucocorticoid excess is one of the most common causes of secondary osteopenia, and several studies have examined the role of miR-29-3p in glucocorticoid-induced bone loss. *In vitro*, supraphysiological doses of glucocorticoids can decrease the expression of miR-29a-3p in the osteoblast lineage (12). Similarly, miR-29a-3p levels in bone are decreased by glucocorticoid excess in both mice and rats (55, 56). In mice globally overexpressing miR-29a-3p under the control of the phosphoglycerate kinase (PGK) promoter, bone loss caused by pharmacologic doses of glucocorticoid was attenuated. This effect appeared to be due to decreased osteoclast number, with a more modest impact on bone formation rate (56, 57). Further, over expression of miR-29a-3p in rats using a lentiviral vector also protected against glucocorticoid mediated osteopenia, demonstrating enhanced bone formation, as well as attenuated osteoclast differentiation in response to glucocorticoid treatment (55).

Another study examined miR-29-3p in estrogen deficiency, which is a prominent cause of post-menopausal bone loss. Here, miR-29a-3p was shown to be down regulated in bone

from mice subjected of ovariectomy (58). In transgenic mice overexpressing miR-29a-3p under the control of the osteocalcin promoter, ovariectomy-induced bone loss was partially rescued. Interestingly, miR-29a-3p overexpression in osteoblasts increased bone formation rate and decreased osteoclast number. *Rankl* was subsequently identified as a novel miR-29-3p target, contributing to an indirect mechanism by which miR-29-3p regulates osteoclast number *in vivo* (58). Although we did not observe a significant increase in *Rankl* mRNA in bone from the miR-29-3p decoy mice, *Opg* mRNA was decreased, resulting in an increased *Rankl/Opg* ratio (Figure 4E), which could favor osteoclast formation. This may be interpreted as a potential compensatory response by the osteoblast lineage to maintain skeletal homeostasis by promoting osteoclast number and function in the face of decreased miR-29-3p activity in osteoclasts, themselves.

Although we did not observe a significant in vivo impact of the miR-29-3p decoy on osteoclast numbers or function under homeostatic conditions or in mice treated with PTH (Figures 3, 6, 8), an inflammatory challenge may illicit a differential response. In mice treated with lipopolysaccharide (LPS), often used to generate an inflammatory response *in vitro* and *in vivo*, levels of miR-29b-3p are increased in bone. In vitro, overexpression of miR-29b-3p in mouse osteoclastic cells promoted survival, whereas inhibition of miR-29b-3p activity was pro-apoptotic. In that study, BCL2 modifying factor, an apoptosis activator, was validated as a novel miR-29-3p target (9). Studies aimed at examining the response of miR-29-3p decoy mice to inflammation are underway.

In bone, expression of miR-29-3p family members is altered in models of inflammatory disease, estrogen deficiency and glucocorticoid excess (9, 55–58). Often, the impact of miR-29-3p on disease phenotype was evaluated when miR-29 family members were overexpressed. However, miRNA overexpression may affect the ability of other miRNAs to access the RISC and/or could lead to the engagement of lower affinity miRNA targets (59). Our approach involved inhibiting miR-29-3p family members using a tough decoy. Expression of the decoy cassette decreased the abundance of miR-29-3p isoforms by 30–60%, a level similar to that seen with other miRNA decoy constructs (15). Sequestration of miRNA-mRNA complexes in P-bodies may also provide additional relief from miRNA targeting (15, 60). Whereas other groups have created mice with targeted deletion of one or both miR-29 loci, studies of the impact on the skeleton have yet to be reported (61–64).

Bone homeostasis is regulated by multiple organs, including brain, gut, kidney, liver and adrenal gland (2), and miR-29-3p family members are broadly, but not ubiquitously, expressed (65–68). Our global miR-29-3p decoy model represents a modest loss-of-function, which could be a very relevant tool for assessing the possible impact of systemic administration of miR-29-3p inhibitors. On the other hand, expression of the miR-29-3p decoy in extra-skeletal tissues may make it more difficult to isolate the role of miR-29-3p in bone cells. Our data provide a strong rationale for additional studies using more lineage or differentiation restricted cre-drivers (i.e. LysM-cre or osteocalcin-cre or DMP1-cre) to activate expression of the miR-29 decoy. This would allow us to better understand the role of miR-29-3p in the osteoclasts, osteoblasts and osteocytes.

Nonetheless, our results demonstrate a differential role for the miR-29-3p family in bone homeostasis vs. intermittent PTH-induced bone anabolism. In osteoporosis patients, PTH injection decreases risk fracture to a much greater extent in vertebral bone than at non-vertebral sites. This is primarily because the positive impact of PTH on trabecular compartment is greater than that for cortical bone (69). In miR-29 decoy mice, intermittent PTH enhanced cortical thickness to a greater extent than in wild type, which may provide a rationale for co-administration of PTH and miR-29-3p inhibitors, to boost bone formation, particularly in the cortical compartment.

Supplementary Material

Refer to Web version on PubMed Central for supplementary material.

Acknowledgements.

The authors thank the UConn Health MicroCT Core facility for assistance with the MicroCT data acquisition, the UConn Heath Center for Regenerative Medicine for use of their microscopy and TD-NMR equipment, and the UConn Health Musculoskeletal Institute for use of their OsteoMeasure software and histology processing equipment. Histomorphometric analysis of bones from PTH treated mice was performed by the Histomorphometry Core Laboratory at the University of California, Los Angeles.

Funding.

This work was supported by the National Institute of Arthritis and Musculoskeletal and Skin Diseases of the National Institutes of Health [AR064867, AMD/SKL]; the National Institutes for Dental and Craniofacial Research [T90DE21989]; and the Center for Molecular Oncology at UConn Health.

References

1. Kapinas K, Delany AM. MicroRNA biogenesis and regulation of bone remodeling. Arthritis research & therapy. 2011;13(3):220. doi: 10.1186/ar3325. [PubMed: 21635717]
2. Zaidi M, Yuen T, Sun L, Rosen CJ. Regulation of Skeletal Homeostasis. Endocrine reviews. 2018;39(5):701–18. Epub 2018/06/14. doi: 10.1210/er.2018-00050. [PubMed: 29897433]
3. Franceschetti T, Kessler CB, Lee SK, Delany AM. miR-29 promotes murine osteoclastogenesis by regulating osteoclast commitment and migration. The Journal of biological chemistry. 2013;288(46):33347–60. Epub 2013/10/03. doi: 10.1074/jbc.M113.484568. [PubMed: 24085298]
4. Smith SS, Dole NS, Franceschetti T, Hrdlicka HC, Delany AM. MicroRNA-433 Dampens Glucocorticoid Receptor Signaling, Impacting Circadian Rhythm and Osteoblastic Gene Expression. J Biol Chem. 2016;291(41):21717–28. Epub 2016/08/24. doi: 10.1074/jbc.M116.737890. [PubMed: 27551048]
5. Li Z, Hassan MQ, Jafferji M, Aqeilan RI, Garzon R, Croce CM, et al. Biological functions of miR-29b contribute to positive regulation of osteoblast differentiation. J Biol Chem. 2009;284(23):15676–84. [PubMed: 19342382]
6. Rossi M, Pitari MR, Amodio N, Di Martino MT, Conforti F, Leone E, et al. miR-29b negatively regulates human osteoclastic cell differentiation and function: implications for the treatment of multiple myeloma-related bone disease. J Cell Physiol. 2013;228(7):1506–15. Epub 2012/12/21. doi: 10.1002/jcp.24306. [PubMed: 23254643]
7. Hrdlicka HC, Lee SK, Delany AM. MicroRNAs are Critical Regulators of Osteoclast Differentiation. Current molecular biology reports. 2019;5(1):65–74. Epub 2019/02/26. doi: 10.1007/s40610-019-0116-3. [PubMed: 30800633]
8. Kriegel AJ, Liu Y, Fang Y, Ding X, Liang M. The miR-29 family: genomics, cell biology, and relevance to renal and cardiovascular injury. Physiol Genomics. 2012;44(4):237–44. [PubMed: 22214600]

9. Sul OJ, Rajasekaran M, Park HJ, Suh JH, Choi HS. MicroRNA-29b Enhances Osteoclast Survival by Targeting BCL-2-Modifying Factor after Lipopolysaccharide Stimulation. Oxidative medicine and cellular longevity. 2019;2019:6018180 Epub 2019/05/17. doi: 10.1155/2019/6018180. [PubMed: 31093317]
10. Kapinas K, Kessler C, Ricks T, Gronowicz G, Delany AM. miR-29 modulates Wnt signaling in human osteoblasts through a positive feedback loop. J Biol Chem. 2010;285(33):25221–31. [PubMed: 20551325]
11. Kapinas K, Kessler CB, Delany AM. miR-29 Suppression of Osteonectin in Osteoblasts: Regulation During Differentiation and by Canonical Wnt Signaling. Journal of cellular biochemistry. 2009;108(1):216–24. doi: 10.1002/jcb.22243. [PubMed: 19565563]
12. Ko JY, Chuang PC, Chen MW, Ke HC, Wu SL, Chang YH, et al. MicroRNA-29a ameliorates glucocorticoid-induced suppression of osteoblast differentiation by regulating beta-catenin acetylation. Bone. 2013;57(2):468–75. Epub 2013/10/08. doi: 10.1016/j.bone.2013.09.019. [PubMed: 24096265]
13. Tan K, Peng YT, Guo P. MiR-29a promotes osteogenic differentiation of mesenchymal stem cells via targeting HDAC4. European review for medical and pharmacological sciences. 2018;22(11):3318–26. Epub 2018/06/20. doi: 10.26355/eurrev_201806_15151. [PubMed: 29917181]
14. Haraguchi T, Ozaki Y, Iba H. Vectors expressing efficient RNA decoys achieve the long-term suppression of specific microRNA activity in mammalian cells. Nucleic acids research. 2009;37(6):e43 Epub 2009/02/19. doi: 10.1093/nar/gkp040. [PubMed: 19223327]
15. Bak RO, Hollensen AK, Primo MN, Sørensen CD, Mikkelsen JG. Potent microRNA suppression by RNA Pol II-transcribed 'Tough Decoy' inhibitors. RNA. 2013;19(2):280–93. doi: 10.1261/rna.034850.112. [PubMed: 23249752]
16. Hollensen AK, Bak RO, Haslund D, Mikkelsen JG. Suppression of microRNAs by dual-targeting and clustered Tough Decoy inhibitors. RNA Biol. 2013;10(3):406–14. Epub 2013/01/18. doi: 10.4161/rna.23543. [PubMed: 23324610]
17. Dole NS, Kapinas K, Kessler CB, Yee SP, Adams DJ, Pereira RC, et al. A single nucleotide polymorphism in osteonectin 3' untranslated region regulates bone volume and is targeted by miR-433. J Bone Miner Res. 2014 Epub 2014/09/30. doi: 10.1002/jbmr.2378.
18. Machado do Reis L, Kessler CB, Adams DJ, Lorenzo J, Jorgetti V, Delany AM. Accentuated osteoclastic response to parathyroid hormone undermines bone mass acquisition in osteonectin-null mice. Bone. 2008;43(2):264–73. [PubMed: 18499553]
19. Xie J, Ameres SL, Friedline R, Hung JH, Zhang Y, Xie Q, et al. Long-term, efficient inhibition of microRNA function in mice using rAAV vectors. Nat Methods. 2012;9(4):403–9. Epub 2012/03/06. doi: 10.1038/nmeth.1903. [PubMed: 22388288]
20. Haraguchi T, Nakano H, Tagawa T, Ohki T, Ueno Y, Yoshida T, et al. A potent 2′ -O- methylated RNA-based microRNA inhibitor with unique secondary structures. Nucleic acids research. 2012;40(8):e58–e. doi: 10.1093/nar/gkr1317. [PubMed: 22259037]
21. Dempster DW, Compston JE, Drezner MK, Glorieux FH, Kanis JA, Malluche H, et al. Standardized nomenclature, symbols, and units for bone histomorphometry: a 2012 update of the report of the ASBMR Histomorphometry Nomenclature Committee. Journal of bone and mineral research : the official journal of the American Society for Bone and Mineral Research. 2013;28(1):2–17. Epub 2012/12/01. doi: 10.1002/jbmr.1805.
22. Ding M, Danielsen CC, Hvid I, Overgaard S. Three-dimensional microarchitecture of adolescent cancellous bone. Bone. 2012;51(5):953–60. doi: 10.1016/j.bone.2012.07.018. [PubMed: 22884723]
23. Deymier AC, Schwartz AG, Lim C, Wingender B, Kotiya A, Shen H, et al. Multiscale effects of spaceflight on murine tendon and bone. Bone. 2020;131:115152 Epub 2019/11/16. doi: 10.1016/j.bone.2019.115152. [PubMed: 31730829]
24. Kozomara A, Birgaoanu M, Griffiths-Jones S. miRBase: from microRNA sequences to function. Nucleic acids research. 2019;47(D1):D155–d62. Epub 2018/11/14. doi: 10.1093/nar/gky1141. [PubMed: 30423142]

25. Griffiths-Jones S, Saini HK, van Dongen S, Enright AJ. miRBase: tools for microRNA genomics. Nucleic acids research. 2008;36(Database issue):D154–8. Epub 2007/11/10. doi: 10.1093/nar/gkm952. [PubMed: 17991681]
26. Griffiths-Jones S, Grocock RJ, van Dongen S, Bateman A, Enright AJ. miRBase: microRNA sequences, targets and gene nomenclature. Nucleic acids research. 2006;34(Database issue):D140–4. Epub 2005/12/31. doi: 10.1093/nar/gkj112. [PubMed: 16381832]
27. Smith SS, Kessler CB, Shenoy V, Rosen CJ, Delany AM. Igf-I 3' untranslated region: strain-specific polymorphisms and motifs regulating igf-I in osteoblasts. Endocrinology. 2013;154(1):253–62. [PubMed: 23183171]
28. Franceschetti T, Dole NS, Kessler CB, Lee S-K, Delany AM. Pathway Analysis of MicroRNA Expression Profile during Murine Osteoclastogenesis. PLOS ONE. 2014;9(9):e107262. doi: 10.1371/journal.pone.0107262. [PubMed: 25222202]
29. Hwang HW, Wentzel EA, Mendell JT. A hexanucleotide element directs microRNA nuclear import. Science (New York, NY). 2007;315(5808):97–100. Epub 2007/01/06. doi: 10.1126/science.1136235.
30. Glatt V, Canalis E, Stadmeyer L, Bouxsein ML. Age-related changes in trabecular architecture differ in female and male C57BL/6J mice. J Bone Miner Res. 2007;22(8):1197–207. [PubMed: 17488199]
31. Glantschnig C, Koenen M, Gil-Lozano M, Karbiener M, Pickrahn I, Williams-Dautovich J, et al. A miR-29a-driven negative feedback loop regulates peripheral glucocorticoid receptor signaling. FASEB journal : official publication of the Federation of American Societies for Experimental Biology. 2019;33(5):5924–41. Epub 2019/02/12. doi: 10.1096/fj.201801385RR. [PubMed: 30742779]
32. Li J, Zuo B, Zhang L, Dai L, Zhang X. Osteoblast versus Adipocyte: Bone Marrow Microenvironment-Guided Epigenetic Control. Case Reports in Orthopedic Research. 2018;1(1):2–18. doi: 10.1159/000489053.
33. Bukowska J, Frazier T, Smith S, Brown T, Bender R, McCarthy M, et al. Bone Marrow Adipocyte Developmental Origin and Biology. Current osteoporosis reports. 2018;16(3):312–9. Epub 2018/04/19. doi: 10.1007/s11914-018-0442-z. [PubMed: 29667012]
34. Zhu Y, Zheng G, Wang H, Jia Y, Zhang Y, Tang Y, et al. Downregulated miR-29a/b/c during Contact Inhibition Stage Promote 3T3-L1 Adipogenesis by Targeting DNMT3A. PLoS One. 2017;12(1):e0170636 Epub 2017/01/24. doi: 10.1371/journal.pone.0170636. [PubMed: 28114345]
35. He A, Zhu L, Gupta N, Chang Y, Fang F. Overexpression of micro ribonucleic acid 29, highly up-regulated in diabetic rats, leads to insulin resistance in 3T3-L1 adipocytes. Molecular endocrinology (Baltimore, Md). 2007;21(11):2785–94. Epub 2007/07/27. doi: 10.1210/me.2007-0167.
36. Wein MN, Kronenberg HM. Regulation of Bone Remodeling by Parathyroid Hormone. Cold Spring Harbor perspectives in medicine. 2018;8(8). Epub 2018/01/24. doi: 10.1101/cshperspect.a031237.
37. Ge M, Liu C, Li L, Lan M, Yu Y, Gu L, et al. miR-29a/b1 Inhibits Hair Follicle Stem Cell Lineage Progression by Spatiotemporally Suppressing WNT and BMP Signaling. Cell Rep. 2019;29(8):2489–504.e4. Epub 2019/11/21. doi: 10.1016/j.celrep.2019.10.062. [PubMed: 31747615]
38. Xiao L, Fei Y, Hurley MM. FGF2 crosstalk with Wnt signaling in mediating the anabolic action of PTH on bone formation. Bone reports. 2018;9:136–44. Epub 2018/09/28. doi: 10.1016/j.bonr.2018.09.003. [PubMed: 30258857]
39. Liu D, Qin H, Yang J, Yang L, He S, Chen S, et al. Different effects of Wnt/β-catenin activation and PTH activation in adult and aged male mice metaphyseal fracture healing. BMC Musculoskelet Disord. 2020;21(1):110 Epub 2020/02/23. doi: 10.1186/s12891-020-3138-3. [PubMed: 32075627]
40. Alford AI, Kozloff KM, Hankenson KD. Extracellular matrix networks in bone remodeling. Int J Biochem Cell Biol. 2015;65:20–31. Epub 05/18. doi: 10.1016/j.biocel.2015.05.008. [PubMed: 25997875]

41. van Rooij E, Sutherland LB, Thatcher JE, DiMaio JM, Naseem RH, Marshall WS, et al. Dysregulation of microRNAs after myocardial infarction reveals a role of miR-29 in cardiac fibrosis. Proc Natl Acad Sci U S A. 2008;105(35):13027–32. Epub 08/22. doi: 10.1073/pnas.0805038105. [PubMed: 18723672]
42. St John HC, Bishop KA, Meyer MB, Benkusky NA, Leng N, Kendziorski C, et al. The osteoblast to osteocyte transition: epigenetic changes and response to the vitamin D3 hormone. Mol Endocrinol. 2014;28(7):1150–65. Epub 2014/06/01. doi: 10.1210/me.2014-1091. [PubMed: 24877565]
43. Zeng Q, Wang Y, Gao J, Yan Z, Li Z, Zou X, et al. miR-29b-3p regulated osteoblast differentiation via regulating IGF-1 secretion of mechanically stimulated osteocytes. Cellular & molecular biology letters. 2019;24:11 Epub 2019/03/28. doi: 10.1186/s11658-019-0136-2. [PubMed: 30915127]
44. Saini V, Marengi DA, Barry KJ, Fulzele KS, Heiden E, Liu X, et al. Parathyroid hormone (PTH)/PTH-related peptide type 1 receptor (PPR) signaling in osteocytes regulates anabolic and catabolic skeletal responses to PTH. J Biol Chem. 2013;288(28):20122–34. Epub 2013/06/05. doi: 10.1074/jbc.M112.441360. [PubMed: 23729679]
45. Delgado-Calle J, Tu X, Pacheco-Costa R, McAndrews K, Edwards R, Pellegrini GG, et al. Control of Bone Anabolism in Response to Mechanical Loading and PTH by Distinct Mechanisms Downstream of the PTH Receptor. J Bone Miner Res. 2017;32(3):522–35. Epub 2016/10/28. doi: 10.1002/jbmr.3011. [PubMed: 27704638]
46. Li C, Xing Q, Yu B, Xie H, Wang W, Shi C, et al. Disruption of LRP6 in osteoblasts blunts the bone anabolic activity of PTH. J Bone Miner Res. 2013;28(10):2094–108. Epub 2013/04/24. doi: 10.1002/jbmr.1962. [PubMed: 23609180]
47. Revollo L, Kading J, Jeong SY, Li J, Salazar V, Mbalaviele G, et al. N-cadherin restrains PTH activation of Lrp6/β-catenin signaling and osteoanabolic action. J Bone Miner Res. 2015;30(2):274–85. Epub 2014/08/05. doi: 10.1002/jbmr.2323. [PubMed: 25088803]
48. St John HC, Meyer MB, Benkusky NA, Carlson AH, Prideaux M, Bonewald LF, et al. The parathyroid hormone-regulated transcriptome in osteocytes: parallel actions with 1,25-dihydroxyvitamin D3 to oppose gene expression changes during differentiation and to promote mature cell function. Bone. 2015;72:81–91. Epub 2014/12/03. doi: 10.1016/j.bone.2014.11.010. [PubMed: 25460572]
49. Inui M, Martello G, Piccolo S. MicroRNA control of signal transduction. Nature Reviews Molecular Cell Biology. 2010;11(4):252–63. doi: 10.1038/nrm2868. [PubMed: 20216554]
50. Bartel DP, Chen C-Z. Micromanagers of gene expression: the potentially widespread influence of metazoan microRNAs. Nature Reviews Genetics. 2004;5(5):396–400. doi: 10.1038/nrg1328.
51. Zhao W, Cheng L, Quek C, Bellingham SA, Hill AF. Novel miR-29b target regulation patterns are revealed in two different cell lines. Sci Rep. 2019;9(1):17449 Epub 2019/11/27. doi: 10.1038/s41598-019-53868-x. [PubMed: 31767948]
52. Wang FS, Chung PC, Lin CL, Chen MW, Ke HJ, Chang YH, et al. MicroRNA-29a protects against glucocorticoid-induced bone loss and fragility in rats by orchestrating bone acquisition and resorption. Arthritis Rheum. 2013;65(6):1530–40. [PubMed: 23529662]
53. Le LT, Swingler TE, Crowe N, Vincent TL, Barter MJ, Donell ST, et al. The microRNA-29 family in cartilage homeostasis and osteoarthritis. Journal of molecular medicine (Berlin, Germany). 2016;94(5):583–96. Epub 2015/12/22. doi: 10.1007/s00109-015-1374-z.
54. Fráguas MS, Eggenschwiler R, Hoepfner J, Schiavinato J, Haddad R, Oliveira LHB, et al. MicroRNA-29 impairs the early phase of reprogramming process by targeting active DNA demethylation enzymes and Wnt signaling. Stem Cell Res. 2017;19:21–30. Epub 2016/12/31. doi: 10.1016/j.scr.2016.12.020. [PubMed: 28038351]
55. Wang FS, Chuang PC, Lin CL, Chen MW, Ke HJ, Chang YH, et al. MicroRNA-29a protects against glucocorticoid-induced bone loss and fragility in rats by orchestrating bone acquisition and resorption. Arthritis and rheumatism. 2013;65(6):1530–40. Epub 2013/03/27. doi: 10.1002/art.37948. [PubMed: 23529662]
56. Ko JY, Chuang PC, Ke HJ, Chen YS, Sun YC, Wang FS. MicroRNA-29a mitigates glucocorticoid induction of bone loss and fatty marrow by rescuing Runx2 acetylation. Bone. 2015;81:80–8. Epub 2015/07/05. doi: 10.1016/j.bone.2015.06.022. [PubMed: 26141838]

57. Wu RW, Lian WS, Chen YS, Kuo CW, Ke HC, Hsieh CK, et al. MicroRNA-29a Counteracts Glucocorticoid Induction of Bone Loss through Repressing TNFSF13b Modulation of Osteoclastogenesis. International journal of molecular sciences. 2019;20(20). Epub 2019/10/20. doi: 10.3390/ijms20205141.
58. Lian W-S, Ko J-Y, Chen Y-S, Ke H-J, Hsieh C-K, Kuo C-W, et al. MicroRNA-29a represses osteoclast formation and protects against osteoporosis by regulating PCAF-mediated RANKL and CXCL12. Cell death & disease. 2019;10(10):705-. doi: 10.1038/s41419-019-1942-1. [PubMed: 31543513]
59. Khan AA, Betel D, Miller ML, Sander C, Leslie CS, Marks DS. Transfection of small RNAs globally perturbs gene regulation by endogenous microRNAs. Nature biotechnology. 2009;27(6):549–55. doi: 10.1038/nbt.1543.
60. Ebert MS, Neilson JR, Sharp PA. MicroRNA sponges: competitive inhibitors of small RNAs in mammalian cells. Nature methods. 2007;4(9):721–6. Epub 08/12. doi: 10.1038/nmeth1079. [PubMed: 17694064]
61. Hu W, Dooley J, Chung SS, Chandramohan D, Cimmino L, Mukherjee S, et al. miR-29a maintains mouse hematopoietic stem cell self-renewal by regulating Dnmt3a. Blood. 2015;125(14):2206–16. Epub 2015/01/31. doi: 10.1182/blood-2014-06-585273. [PubMed: 25634742]
62. Papadopoulou AS, Serneels L, Achsel T, Mandemakers W, Callaerts-Vegh Z, Dooley J, et al. Deficiency of the miR-29a/b-1 cluster leads to ataxic features and cerebellar alterations in mice. Neurobiology of disease. 2015;73:275–88. Epub 2014/10/16. doi: 10.1016/j.nbd.2014.10.006. [PubMed: 25315682]
63. Takeda T, Tanabe H. Lifespan and reproduction in brain-specific miR-29-knockdown mouse. Biochemical and biophysical research communications. 2016;471(4):454–8. Epub 2016/02/24. doi: 10.1016/j.bbrc.2016.02.055. [PubMed: 26902119]
64. Cushing L, Costinean S, Xu W, Jiang Z, Madden L, Kuang P, et al. Disruption of miR-29 Leads to Aberrant Differentiation of Smooth Muscle Cells Selectively Associated with Distal Lung Vasculature. PLoS genetics. 2015;11(5):e1005238 Epub 2015/05/29. doi: 10.1371/journal.pgen.1005238. [PubMed: 26020233]
65. Papatheodorou I, Moreno P, Manning J, Fuentes AM-P, George N, Fexova S, et al. Expression Atlas update: from tissues to single cells. Nucleic acids research. 2019;48(D1):D77–D83. doi: 10.1093/nar/gkz947.
66. de Rie D, Abugessaisa I, Alam T, Arner E, Arner P, Ashoor H, et al. An integrated expression atlas of miRNAs and their promoters in human and mouse. Nature Biotechnology. 2017;35(9):872–8. doi: 10.1038/nbt.3947.
67. Lagos-Quintana M, Rauhut R, Yalcin A, Meyer J, Lendeckel W, Tuschl T. Identification of Tissue-Specific MicroRNAs from Mouse. Current Biology. 2002;12(9):735–9. doi: 10.1016/S0960-9822(02)00809-6. [PubMed: 12007417]
68. Ludwig N, Leidinger P, Becker K, Backes C, Fehlmann T, Pallasch C, et al. Distribution of miRNA expression across human tissues. Nucleic acids research. 2016;44(8):3865–77. doi: 10.1093/nar/gkw116. [PubMed: 26921406]
69. Baron R, Hesse E. Update on bone anabolics in osteoporosis treatment: rationale, current status, and perspectives. J Clin Endocrinol Metab 2012 2;97(2):311–25. doi: 10.1210/jc.2011-2332 [PubMed: 22238383]

Highlights

- The miR-29 family promotes osteoblast and osteoclast differentiation in vitro.
- Mice globally expressing a miR-29-3p tough decoy have decreased trabecular bone volume.
- In bone homeostasis, the miR-29-3p decoy suppresses bone formation.
- In contrast, the miR-29-3p decoy augmented intermittent PTH mediated bone anabolism.
- miR-29-3p plays a differential role in basal vs. PTH-mediated bone formation.

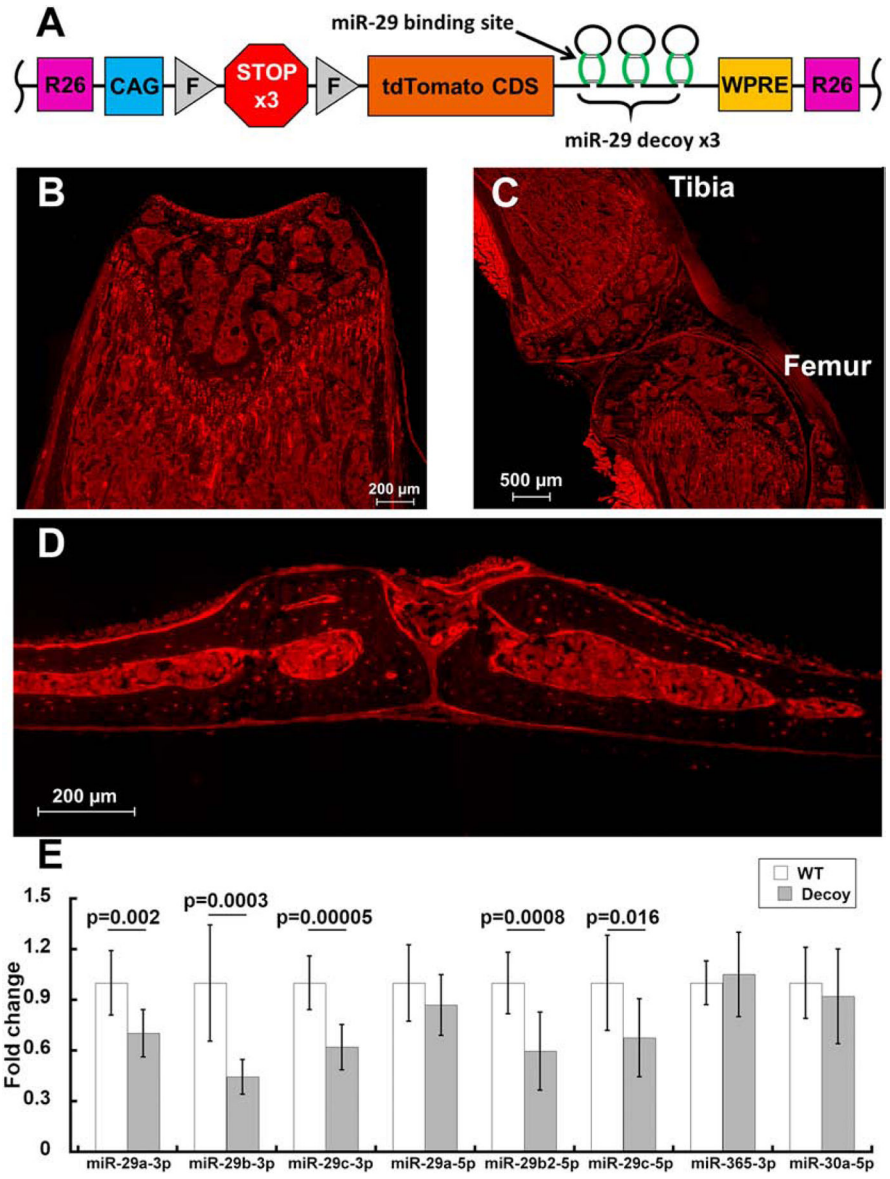

Figure 1. Global miR-29 decoy mice.

(**A**) Schematic of the miR-29-3p decoy cassette that was knocked into the Rosa26 locus of C57BL/6 mice. It consists of the CAG promoter, three copies of a transcription stop sequence flanked by Loxp sites (F), and the coding sequence for tdTomato (red fluorescent reporter), with three copies of a miR-29 tough decoy in its 3'-UTR. Each tough decoy contains two miR-29 binding sites (in green). WPRE was added to enhance expression of the decoy. (**B-D**) Representative images of tdTomato fluorescence in bone from two-month-old mice: femur (**B**), knee joint (**C**), and calvarium (**D**). (**E**) Expression of miR-29 isoforms and other miRNAs in calvaria from 2-month-old female wild-type and global miR-29 decoy mice. WT n=9; Decoy n=9.

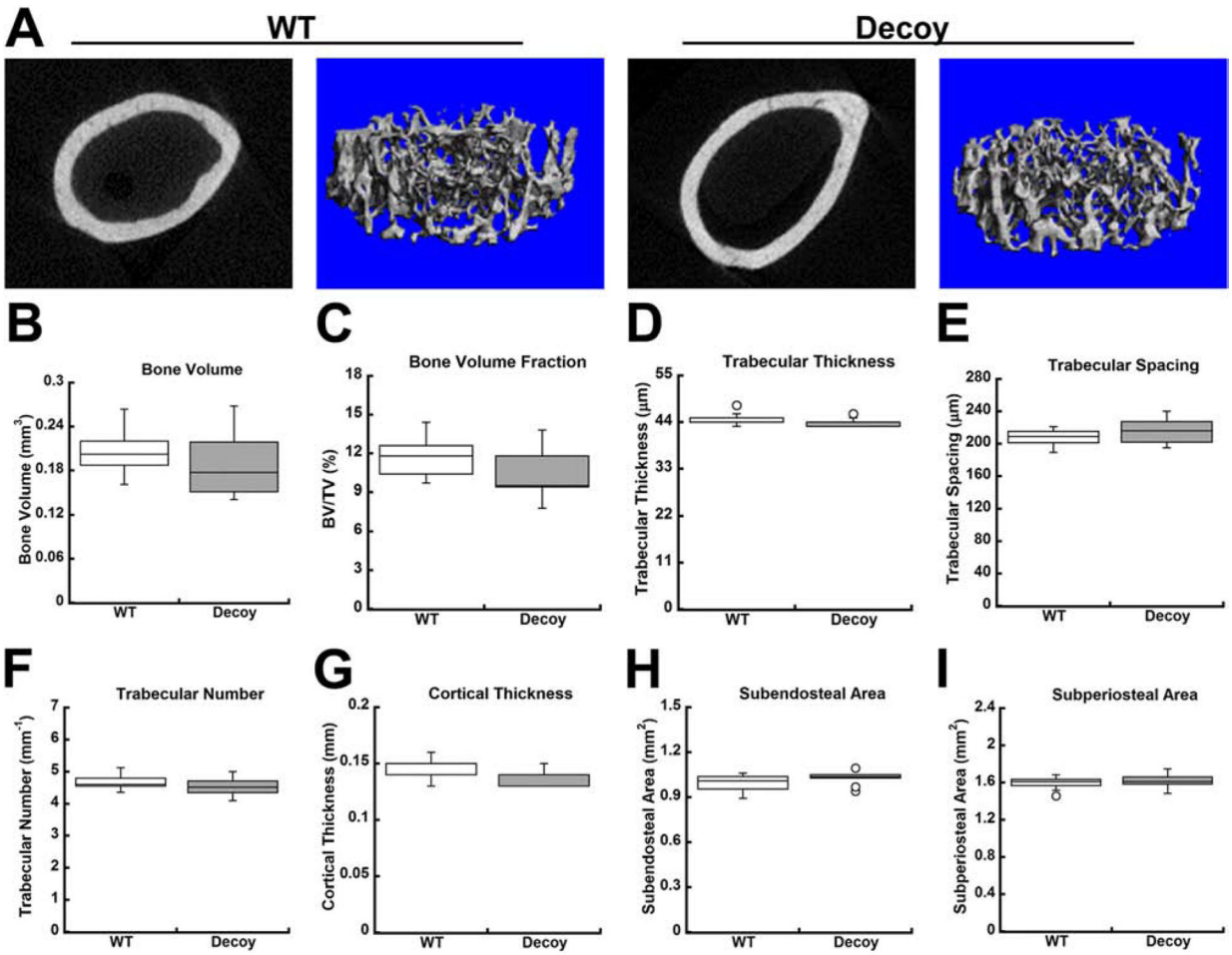

Figure 2. microCT analysis of femoral bone microarchitecture in two-month-old female wild-type and global miR-29 decoy mice.

(**A)** Representative reconstructed images of cortical and trabecular bone. (**B-F**) Quantified trabecular bone parameters: bone volume (**B**), bone volume fraction (BV/TV; bone volume/total volume) (**C**), trabecular thickness (**D**), trabecular spacing (**E**), and trabecular number (**F**). (**G-I**) Quantified cortical bone parameters: cortical thickness (**G**), subendosteal area (**H**), and subperiosteal area (**I**). WT n=17; Decoy n=9.

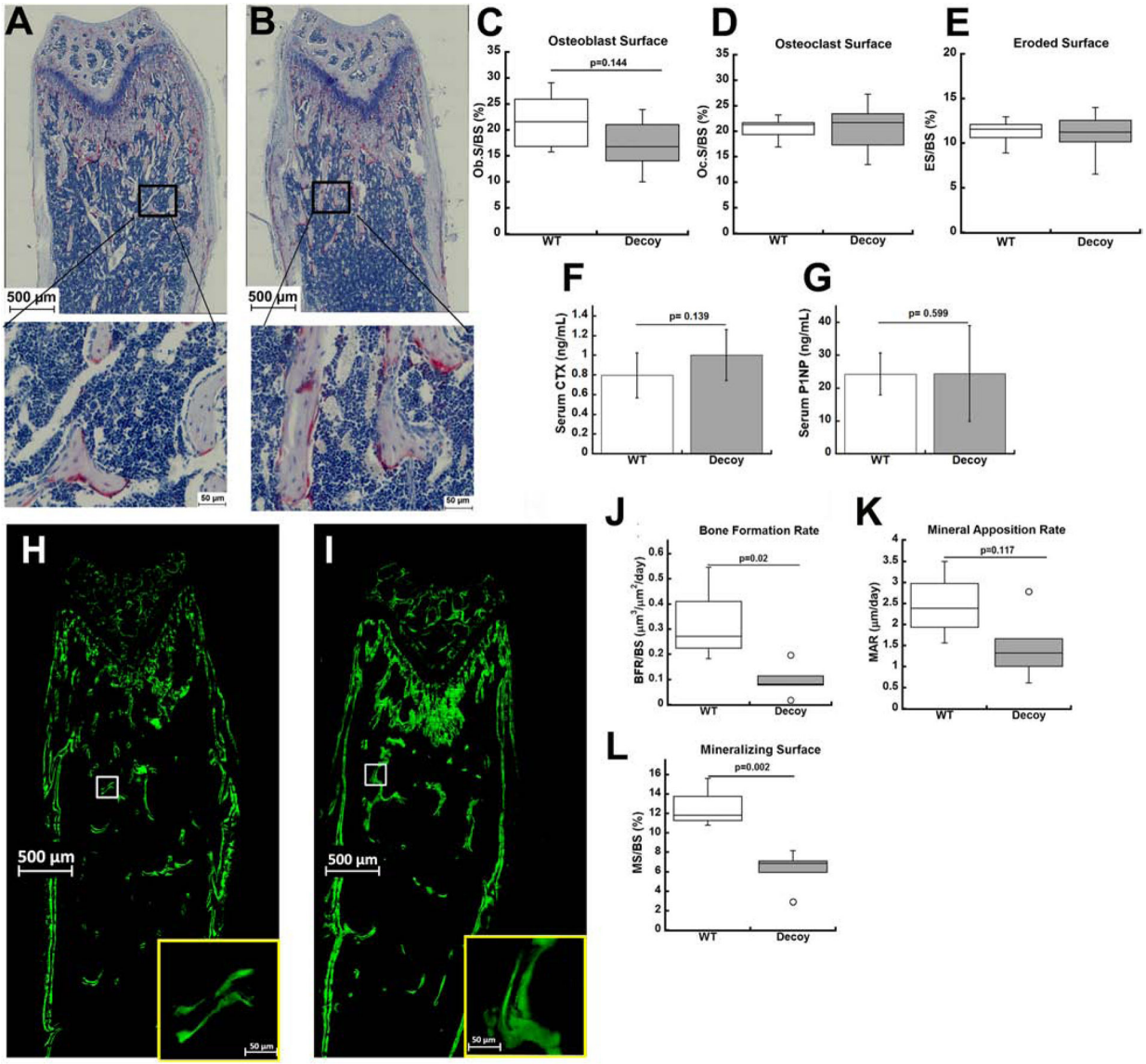

Figure 3. Histomorphometric analysis of femurs from two-month-old wild-type and global miR-29 decoy mice.

(**A, B**) Representative images of TRAP stained sections from wild-type (**A**) and global miR-29 decoy (**B**) mice used for static histomorphometry. (**H, I**) Representative images of calcein-double labeling in wild-type (**H**) and global miR-29 decoy (**I**) mice used for dynamic histomorphometry. (**C-E**) Static histomorphometry measurement of osteoblast surface (**C**), osteoclast surface (**D**), eroded surface (**E**); n=7 for both genotypes. Serum markers of bone remodeling, serum CTX (**F**) and serum P1NP (**G**) were measured by ELISA. WT n=6–7; Decoy n=7. (**J-K**) Dynamic histomorphometry measurement of bone formation rate (**J**), and mineral apposition rate (**K**), mineralizing surface (**L**); WT n=4; Decoy n=5.

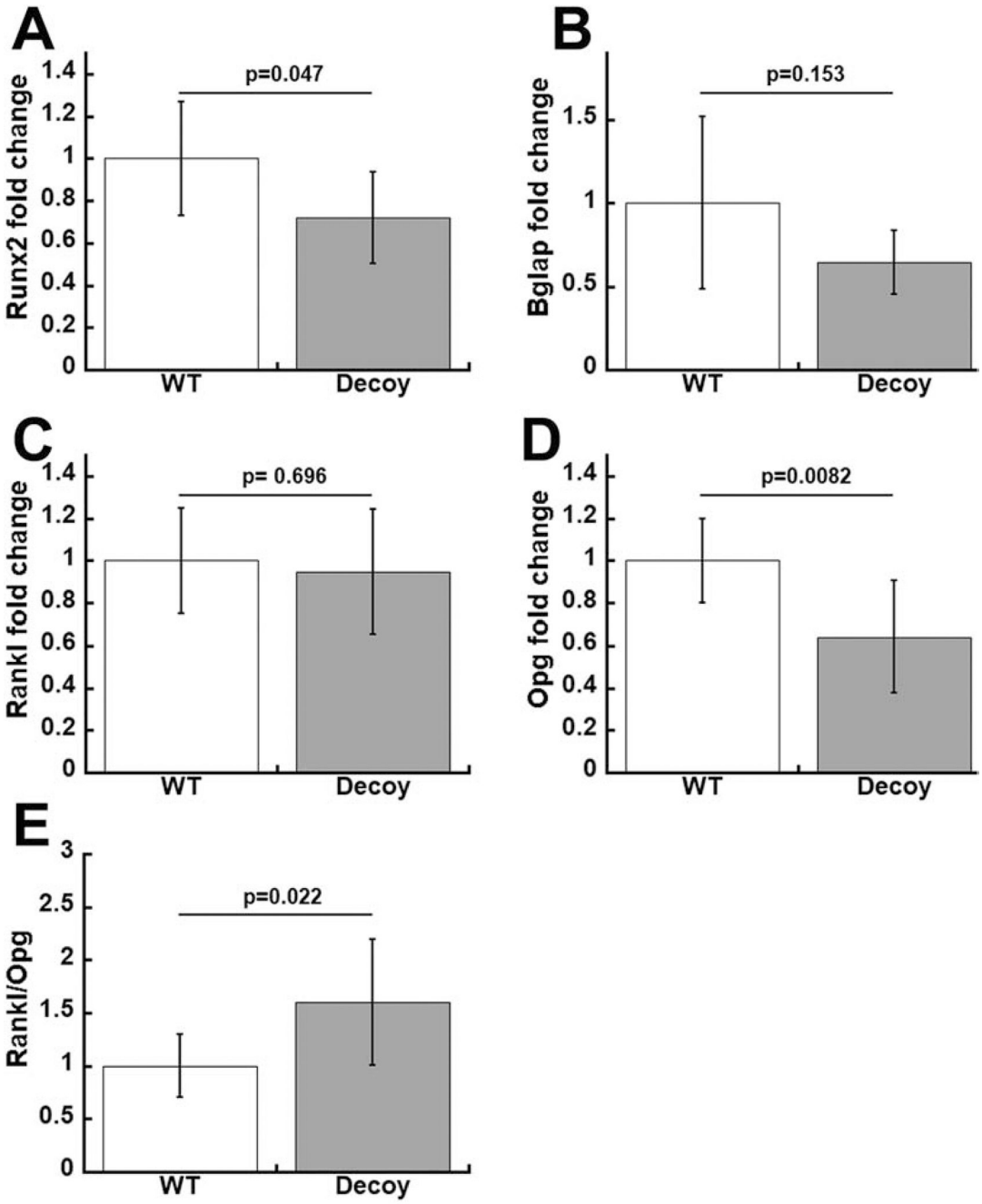

Figure 4. Expression of osteoblastic genes in calvaria from two-month-old global miR-29 decoy mice.

(**A, B**) mRNA for osteoblast marker genes *Runx2* (**A**) and *Bglap* (osteocalcin) (**B**) (**C**-**E**) mRNA for *Rankl* (**C**), *Opg* (**D**), and the *Rankl/Opg* ratio (**E**). n=8 for both genotypes.

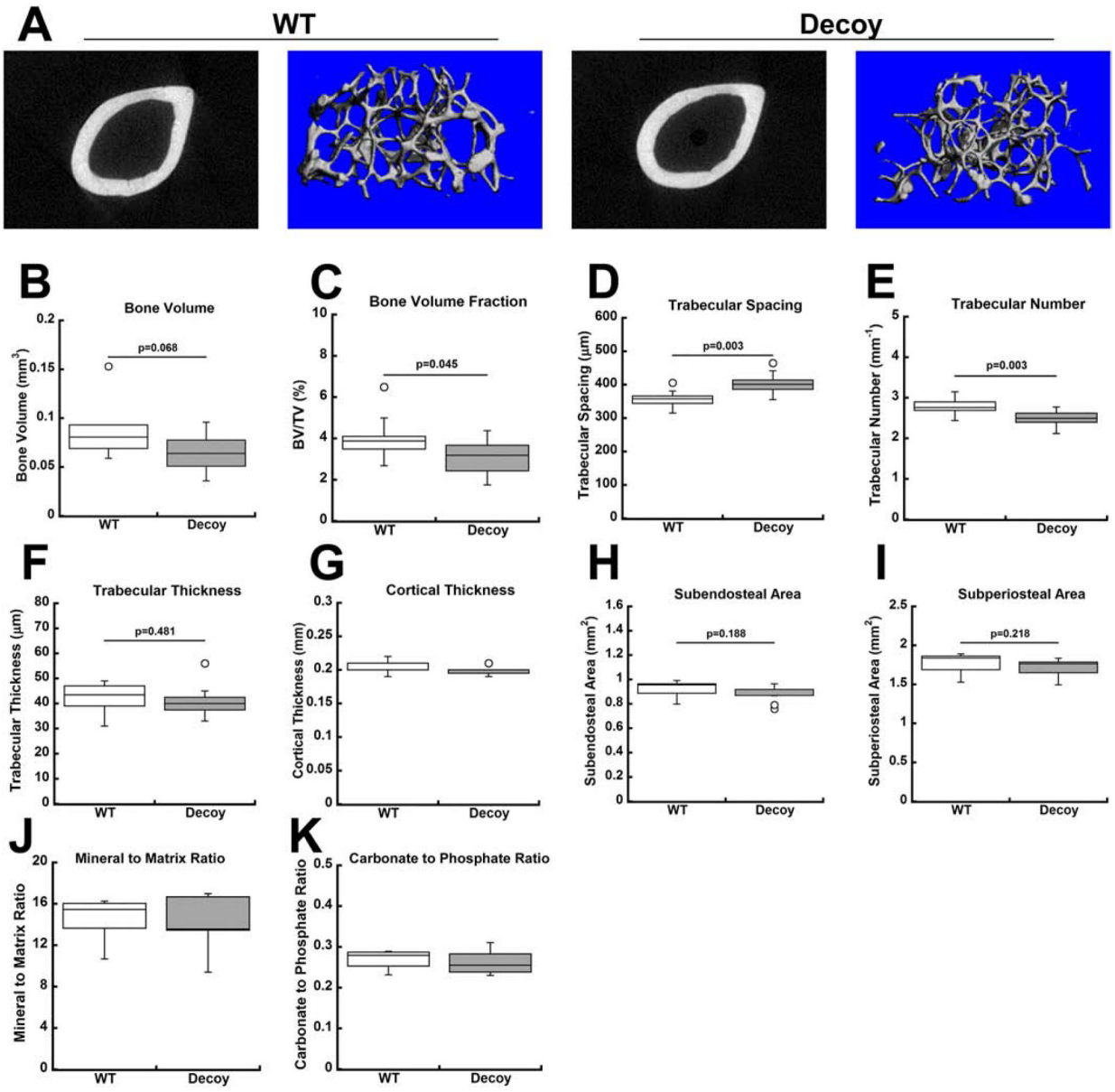

Figure 5. microCT analysis of femoral bone microarchitecture in six-month-old wild-type and global miR-29 decoy mice.

(**A)** Representative reconstructed images of cortical and trabecular bone. (**B-F**) Quantified trabecular bone parameters: bone volume (**B**), bone volume fraction (BV/TV; bone volume/ total volume) (**C**), trabecular spacing (**D**), trabecular number (**E**), and trabecular thickness (**F**). (**G-I**) Quantified cortical bone parameters: cortical thickness (**G**), subendosteal area (**H**), and subperiosteal area (**I**). WT n=10; Decoy n=11. Cortical bone mineral-to-matrix ratio (**J**) and the carbonate-to-phosphate ratio (**K**) in bone sections from 5 month-old mice was determined by Raman spectroscopy; n=5 for both genotypes.

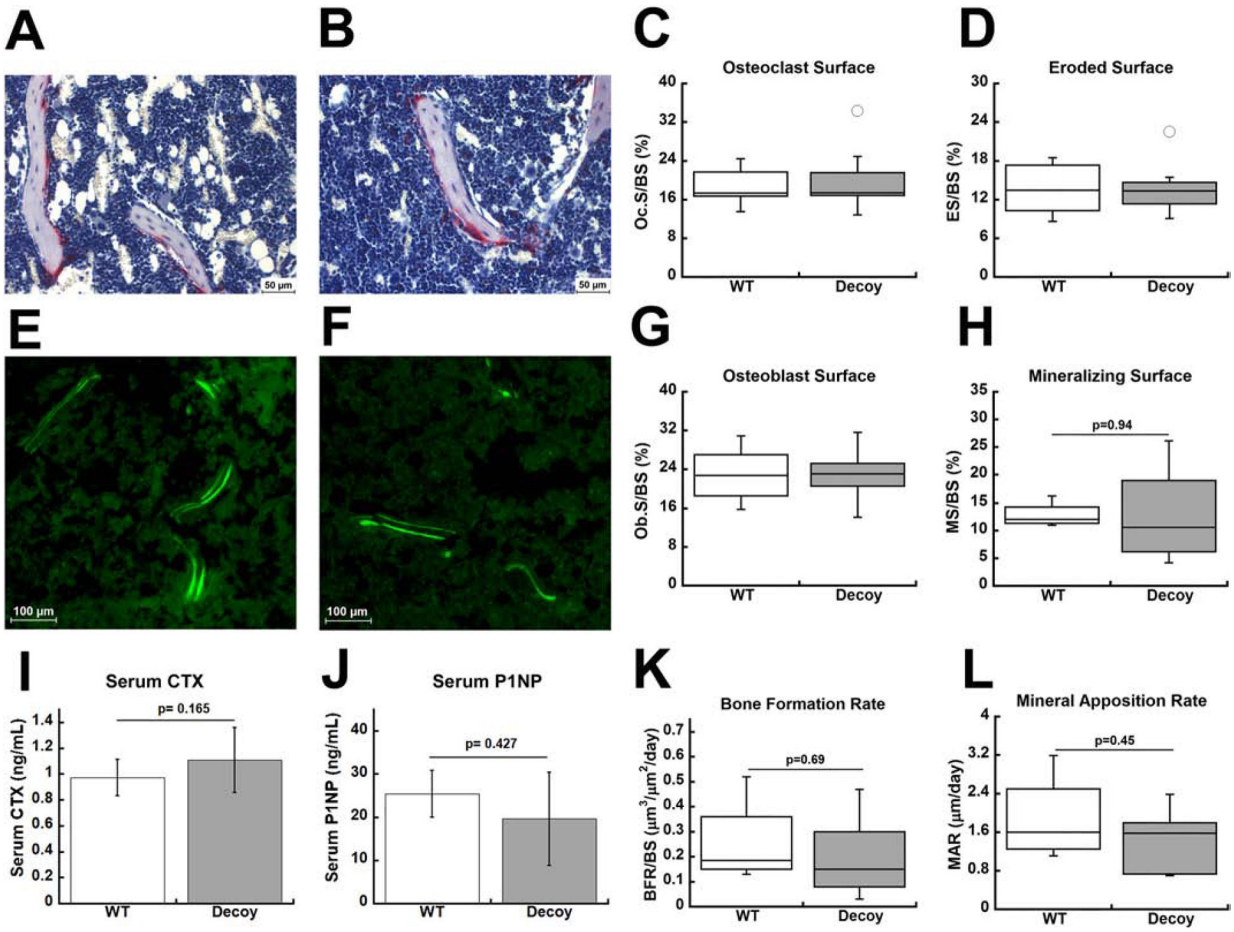

Figure 6. Histomorphometric analysis of femurs from six-month-old wild-type and global miR-29 decoy mice.

(**A, B**) Representative images of TRAP stained sections from wild-type (**A**) and global miR-29 decoy (**B**) mice used for static histomorphometry. (**E, F**) Representative images of calcein-double labeling in wild-type (**E**) and global decoy (**F**) mice used for dynamic histomorphometry. (**C, D, G**) Static histomorphometry measurement of osteoclast surface (**C**), eroded surface (**D**), and osteoblast surface (**G**); WT n=10; Decoy n=11. (**H, K, L**) Dynamic histomorphometry measurement of mineralizing surface (**H**), bone formation rate (**K**), and mineral apposition rate (**L**); WT n=4; Decoy n=5. (**K, L**) Serum markers of bone remodeling, serum CTX (**I**) and serum P1NP (**J**) were measured by ELISA. WT n=8–9; Decoy n=8–11.

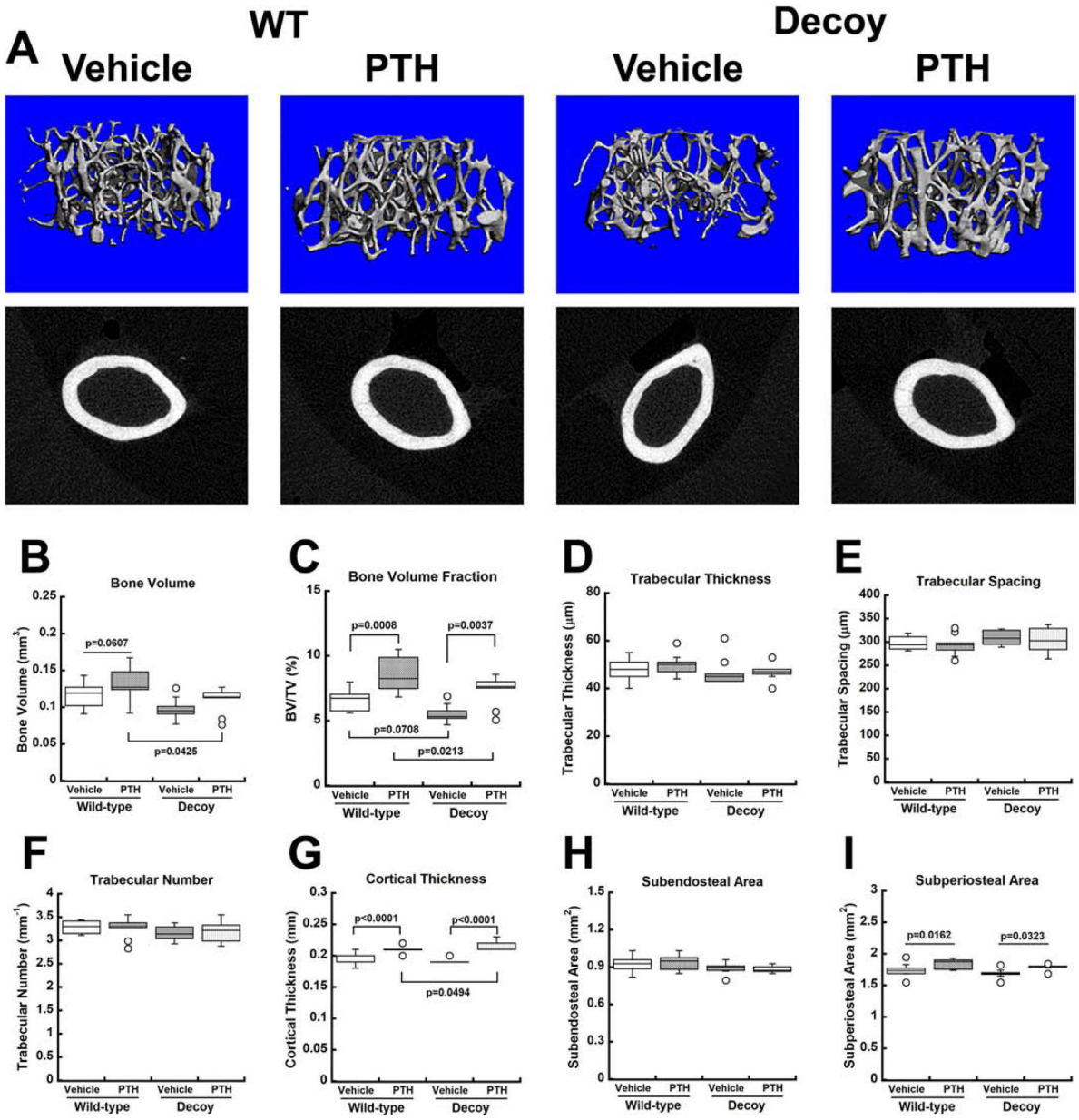

Figure 7. microCT analysis of femoral bone microarchitecture in wild-type and global miR-29 decoy mice treated with intermittent PTH1-34.

(**A)** Representative reconstructed images of trabecular and cortical bone. (**B-F**) Quantified trabecular bone parameters: bone volume (**B**), bone volume fraction (BV/TV; bone volume/ total volume) (**C**), trabecular thickness (**D**), trabecular spacing (**E**), and trabecular number (**F**). (**G-I**) Quantified cortical bone parameters: cortical thickness (**G**), subendosteal area (**H**), and subperiosteal area (**I**). n=9 for all groups.

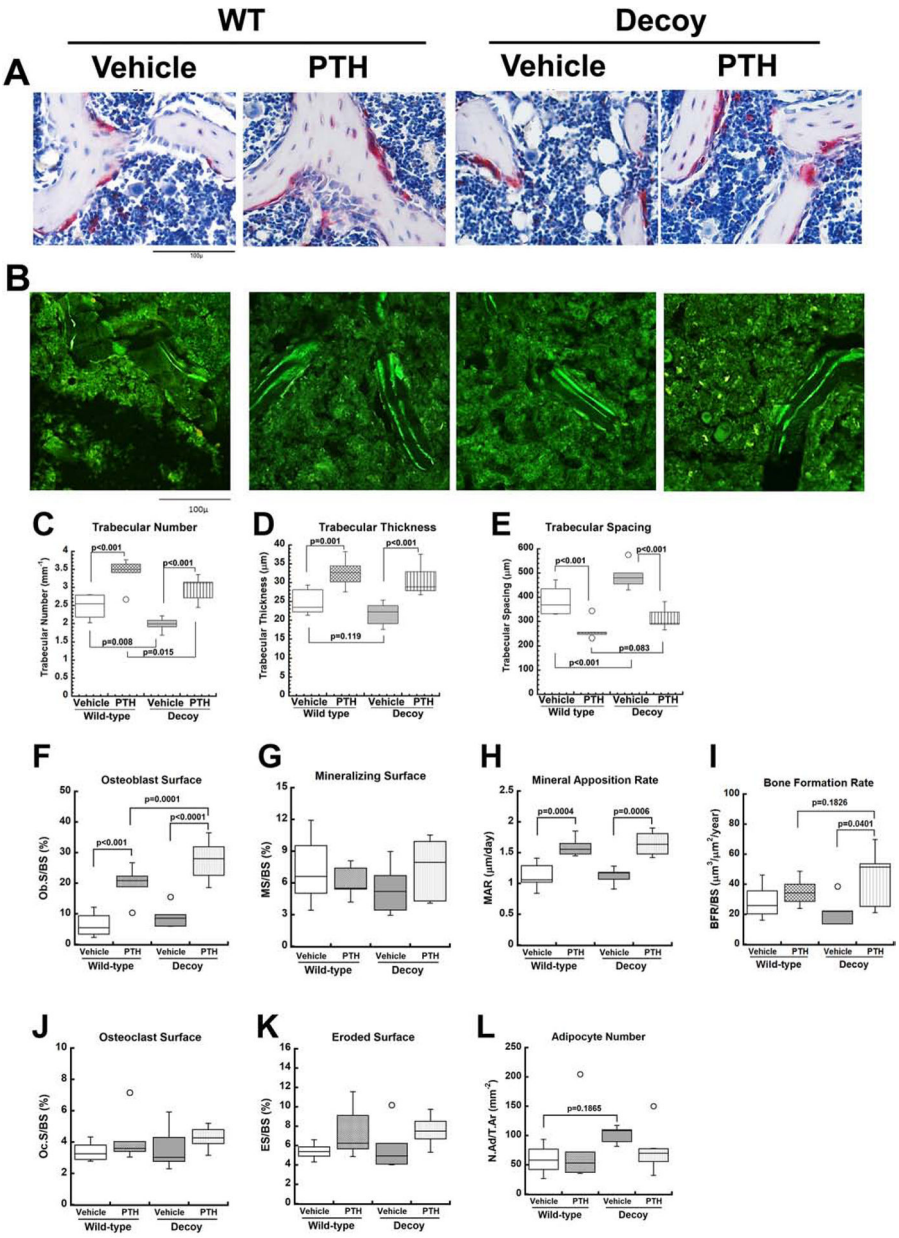

Figure 8. Histomorphometric analysis of femurs from wild-type and global miR-29 decoy mice treated with intermittent PTH1-34.

(**A**) Representative images of TRAP stained sections from wild-type and global miR-29 decoy mice used for static histomorphometry. (**B**) Representative images of calcein-double labeling in wild-type and global decoy mice used for dynamic histomorphometry. (**C-E, J-L)** Static histomorphometry measurement of trabecular number (**C**), trabecular thickness (**D**), trabecular spacing (**E**), osteoblast surface (**F**), osteoclast surface (**J**), eroded surface (**K**), and adipocyte number (**L**). WT vehicle n=8, WT PTH n=6, Decoy vehicle n=6, Decoy PTH n=7. (**G-I**), Dynamic histomorphometry measurement of mineralizing surface (**G**), mineral apposition rate (**H**) and bone formation rate (**I**). WT vehicle n=5, WT PTH n=6, Decoy vehicle n=5, Decoy PTH n=6

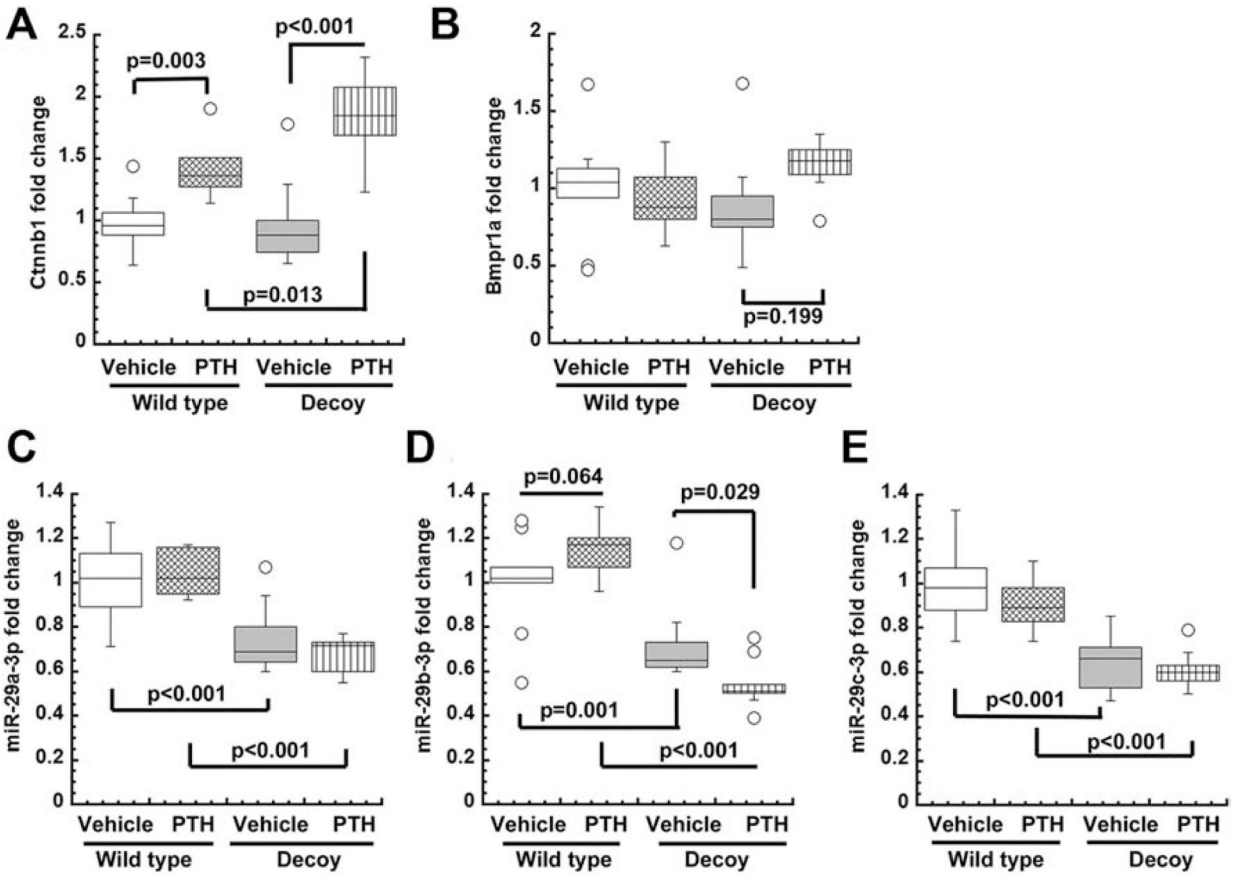

Figure 9. Expression of selected miR-29 targets and miR-29-3p isoforms in calvaria from wild-type and global miR-29 decoy mice treated with intermittent PTH1-34.

(**A, B**) mRNA for miR-29 targets *Ctnnb1* and *Bmpr1a*. (**C**) miR-29a-3p, (**D**) miR-29b-3p, (**E**) miR-29c-3p. n=9 for all groups.